

# Journal of Astronomical Telescopes, Instruments, and Systems

AstronomicalTelescopes.SPIEDigitalLibrary.org

## High-energy photon polarimeter for astrophysics

Maxim Eingorn  
Lakma Fernando  
Branislav Vlahovic  
Cosmin Ilie  
Bogdan Wojtsekhowski  
Guido Maria Urciuoli  
Fulvio De Persio  
Franco Meddi  
Vladimir Nelyubin

**SPIE.**

Maxim Eingorn, Lakma Fernando, Branislav Vlahovic, Cosmin Ilie, Bogdan Wojtsekhowski, Guido Maria Urciuoli, Fulvio De Persio, Franco Meddi, Vladimir Nelyubin, "High-energy photon polarimeter for astrophysics," *J. Astron. Telesc. Instrum. Syst.* **4**(1), 011006 (2018), doi: 10.1117/1.JATIS.4.1.011006.

# High-energy photon polarimeter for astrophysics

Maxim Eingorn,<sup>a</sup> Lakma Fernando,<sup>a</sup> Branislav Vlahovic,<sup>a,\*</sup> Cosmin Ilie,<sup>b,c</sup> Bogdan Wojtsekhowski,<sup>d,\*</sup> Guido Maria Urciuoli,<sup>e</sup> Fulvio De Persio,<sup>e</sup> Franco Meddi,<sup>e,f</sup> and Vladimir Nelyubin<sup>g</sup>

<sup>a</sup>North Carolina Central University, Physics Department, Durham, North Carolina, United States

<sup>b</sup>Colgate University, Department of Physics and Astronomy, Hamilton, New York, United States

<sup>c</sup>National Institute for Physics and Nuclear Engineering, Department of Theoretical Physics, Magurele, Romania

<sup>d</sup>Thomas Jefferson National Accelerator Facility, Newport News, Virginia, United States

<sup>e</sup>INFN, Sezione di Roma, Rome, Italy

<sup>f</sup>Sapienza Università di Roma, Department of Physics, Rome, Italy

<sup>g</sup>University of Virginia, Physics Department, Charlottesville, Virginia, United States

**Abstract.** A high-energy photon polarimeter for astrophysics studies in the energy range from 10 to 800 MeV is considered. The proposed concept uses a stack of silicon microstrip detectors, where they play the roles of both a converter and a tracker. The purpose of this paper is to outline the parameters of such a polarimeter and to estimate the productivity of measurements. Our study, supported by a Monte Carlo simulation, shows that with a 1-year observation period the polarimeter will provide 6% accuracy of the polarization degree for photon energies above 100 MeV, which would be a significant advance relative to the currently explored energy range of a few MeV. The proposed polarimeter design could easily be adjusted to the specific photon energy range to maximize efficiency if needed. © The Authors. Published by SPIE under a Creative Commons Attribution 3.0 Unported License. Distribution or reproduction of this work in whole or in part requires full attribution of the original publication, including its DOI. [DOI: [10.1117/1.JATIS.4.1.011006](https://doi.org/10.1117/1.JATIS.4.1.011006)]

Keywords: gamma ray; pair production; polarimeter; silicon microstrip detector.

Paper 17096SS received Nov. 28, 2017; accepted for publication Mar. 9, 2018; published online Mar. 30, 2018.

## 1 Introduction

Recent discoveries have underlined a key role of astrophysics in the study of nature. We are presenting a potential instrument for measuring high-energy photon polarization with a proven detector technique that should allow preparation of a reliable tool for a future spaceborne observatory.

Polarization of the photon has played an important role (sometimes even before it was recognized) in physics discoveries such as the famous Young's interference experiment,<sup>1</sup> Michelson–Morley's test of the Ether theory,<sup>2</sup> determination of the neutral pion parity,<sup>3,4</sup> and many others, including more recently the spin structure of the nucleon.<sup>5</sup> Polarization of the cosmic microwave background (CMB) will likely be a crucial observable for the inflation theory. (See PLANCK<sup>6</sup> results for constraints on inflationary models based on nondetection of B-modes and Ref. 7 for a review.)

During the last decade, observations from the AGILE<sup>8</sup> and FERMI-LAT<sup>9</sup> pair production telescopes have enhanced our understanding of gamma ( $\gamma$ ) ray astronomy. With the help of these telescopes, numerous high-energy  $\gamma$ -ray sources have been observed. However, the current measurements are insufficient to fully understand the physics mechanism of such  $\gamma$ -ray sources as gamma-ray bursts (GRBs), active galactic nuclei (AGNs), blazars, pulsars, and supernova remnants (SNRs). Even though both telescopes cover a wide range of energy (from 20 MeV to more than 300 GeV), neither of them is capable of sufficiently accurate polarization measurements (recently the authors of Ref. 10 estimated that a  $5\sigma$  minimum detectable polarization of  $\sim 30$  to 50% could be detected by FERMI-LAT for the brightest  $\gamma$  ray

sources only after 10 years of observation) that could shed light on the numerous open problems in medium- to high-energy  $\gamma$  ray astrophysics. For example, precise measurements of ray polarization for  $\gamma$  rays could be used, in principle, to determine the nature of the emission mechanisms responsible for blazars, GRBs, x-ray binaries, pulsars, and magnetars. Moreover, measurements of  $\gamma$ -ray polarization from distant sources such as blazars or GRBs can help address problems in fundamental physics, such as Lorentz invariance.<sup>11</sup>

There are several medium- to high-energy photon polarimeters for astrophysics proposed in the literature. For example, both the NASA Group<sup>12</sup> and the Ecole Polytechnique Group<sup>13,14</sup> are considering Ar(Xe)-based gas-filled detectors: the time projection chamber (TPC) with a microwell or micromega section for amplification of ionization. Similarly, the advanced energetic pair telescope (AdEPT), proposed in Ref. 15, is a pair production telescope capable of polarization measurements using a three-dimensional track imager based on a low-density gaseous (Ar) TPC. Most recently, e-Astrogam<sup>16</sup> has been proposed as a  $\gamma$ -ray space instrument for the fifth medium-sized mission of the European Space Agency. In contrast to the proposals previously mentioned, by the NASA and Ecole Polytechnique Groups, e-Astrogam is based on double-sided silicone strip detectors, allowing high resolution and good sensitivity to linear polarization over its entire bandwidth, from 0.15 MeV to 3 GeV. We evaluate the features of an electron-positron pair polarimeter for the full energy range from 20 to 1000 MeV and then propose a specific design for a polarimeter in the 100 to 300 MeV energy range using silicon microstrip detectors (MSDs) whose principal advantage with respect to the gas-based TPC is that the spatial and two-track resolution is about 5 to 10 times better.

The paper is organized in the following way: in Sec. 2, we briefly discuss the motivation for cosmic  $\gamma$ -ray polarimetry in the high-energy region. Section 3 is devoted to measurement

\*Address all correspondence to: Branislav Vlahovic, E-mail: [vlahovic@nccu.edu](mailto:vlahovic@nccu.edu); Bogdan Wojtsekhowski, E-mail: [bogdanw@jlab.org](mailto:bogdanw@jlab.org)

techniques, polarimeters being built and current proposals. In Sec. 4, we calculate the photon flux coming from the crab pulsar and crab nebula. The design of the new polarimeter and its performance are discussed in the last few sections.

## 2 Scientific Motivation

There are several recent reviews of photon polarimetry in astrophysics,<sup>17–23</sup> which address many questions open for decades that could find a solution via  $\gamma$ -ray polarization measurements. We will briefly discuss those problems in this section. Photon polarimetry for energy below a few MeV is a very active field of astrophysical research, and some examples of the productive use of polarimetry at these energies include detection of exoplanets, analysis of chemical composition of planetary atmosphere, and investigation into interstellar matter, quasar jets, and solar flares. However, no polarization measurements are available in the medium- and high-energy regions ( $\sim 1$  MeV to 1 GeV) because of the instrumental challenges.

The primary motivation in proposing a polarimeter is our interest in understanding the emission and production mechanisms for polarized  $\gamma$  rays in pulsars, GRBs, and AGNs by measuring polarization of cosmic  $\gamma$  rays in this under-explored energy region ( $\sim 100$  to 1000 MeV). Additionally, the polarization observations from the rotation-powered and accretion-powered pulsar radiation mechanisms could help to confirm the identification of black hole candidates.<sup>24</sup>

Polarization measurements could reveal one of the possible effects induced by quantum gravity, the presence of small, but potentially detectable, Lorentz or CPT violating terms in the effective field theory. These terms lead to a macroscopic birefringence effect of the vacuum (see Ref. 25 for more information). Up to now, the highest energy linear polarization measurement has been for GRB 061122 in the 250- to 800-keV energy range,<sup>26</sup> and vacuum birefringence has not been observed in that region. Therefore, extending polarization sensitivity to higher energies could lead to detection of vacuum birefringence, which would have an extraordinary impact on fundamental physics, or in the case of null detection we could significantly improve the present limits on the Lorentz invariance violation parameter.

Further, according to the observations by the Energetic Gamma Ray Experiment Telescope,<sup>27</sup> the synchrotron emission of the crab nebula is significant in the energy below  $\sim 200$  MeV.<sup>28</sup> Additionally, the theoretical studies state that most of the  $\gamma$  rays coming from the crab nebula around 100 MeV may come from its inner knot,<sup>29</sup> so the observations in the neighborhood of 100 MeV will help to test this theoretical hypothesis and confirm the emission mechanism. In 2007, AGILE and Fermi detected strong  $\gamma$ -ray flares originating from the crab system, with a precise localization and physical origin yet to be determined. Future polarization measurements will be crucial in answering those two questions, as they can be used to determine the morphology of the region where particle acceleration takes place.

It is also worth mentioning that polarimetry could test the theories assuming existence of axions (hypothetical particles introduced to solve the strong CP problem of QCD). It is interesting that the same axions or axion-like particles can serve as a foundation for a relevant mechanism of Sun luminosity.<sup>30</sup> A theoretical study<sup>31</sup> has shown that polarization observations from GRBs can be used to constrain the axion-photon coupling  $g_{a\gamma\gamma} \leq 2.2 \times 10^{-11} \text{ GeV}^{-1}$  for the axion mass of  $10^{-3}$  eV.

The limit on the coupling scales is  $\propto 1/\sqrt{E}$ ; therefore, the polarimetry of GRBs at higher energies would lead to tighter constraints.

In the following two sections, we will briefly explain how polarization measurements are involved in confirming the emission mechanism and geometry of two above-mentioned sources.

### 2.1 Pulsars

Pulsars are a type of neutron star, yet they are highly magnetized and rotate at enormous speeds. The questions concerning the way magnetic and electric fields are oriented, how particles are accelerated, and how the energy is converted into radio and  $\gamma$  rays in pulsars are still not fully answered. Because of the extreme conditions in pulsars' interiors, they can be used to understand poorly known properties of superdense, strongly magnetized, and superconducting matter.<sup>32,33</sup> Moreover, by studying pulsars one can learn about the nuclear reactions and interactions between the elementary particles under these conditions, which cannot be reproduced in terrestrial laboratories. Particle acceleration in the polar region of the magnetic field results in  $\gamma$  radiation, which is expected to have a high degree of polarization.<sup>34</sup> Depending on the place where the radiation occurs, the pulsar emission can be explained in the framework of a polar cap model or an outer cap model. In both models, the emission mechanism is similar, but polarization is expected to be dissimilar;<sup>35</sup> hence, polarimetry could be used to understand the pulsar's emission mechanism.

### 2.2 Gamma Ray Bursts

Polarization measurements would also help to understand GRBs. GRBs (see Ref. 36 for a review) are short and extremely bright bursts of  $\gamma$  rays. Usually, a short-time (from  $10^{-3}$  s to about  $10^3$  s) peak of radiation is followed by a long-lasting afterglow. The characteristics of the radiation emitted during the short-time peak and during the afterglow are different. The number of high-energy photons that may be detected during the short-time burst phase is expected to be small compared with the one for the long-lived emission. Although only about 3% of the energy emitted during the short-time burst is carried by high-energy photons with  $E > 100$  MeV, the high-energy photons of the afterglow carry about half of the total emitted energy. Therefore, there is a possibility of observing polarization of high-energy photons during the afterglow. The emission mechanism of GRBs, the magnetic composition, and the geometry and morphology of GRB jets are still uncertain but can be at least partly revealed in this way. For example, in the case of synchrotron emission, the variation of the observed GRB polarization with viewing angle depends strongly on the degree of order of the magnetic fields.

It is worth noting that several studies have discussed how the degree of polarization,  $P$ , depends on the GRB emission mechanisms. In one example, using Monte Carlo methods, Toma et al.<sup>37</sup> showed that the Compton drag model is favored when the degree of polarization  $P > 80\%$  and  $P \sim 20\%$  to  $70\%$  concerns the synchrotron radiation with the ordered magnetic fields model. Moreover, studies by Mundell et al.<sup>38</sup> and Lyutikov et al.<sup>39</sup> have proven that polarimetry could assist in revealing the geometry of GRB jets.

### 2.3 Active Galactic Nuclei

Most galaxies contain a supermassive black hole, which can power, via accretion and other related astrophysical processes, a compact very bright source with strong emission in the optical band, i.e., an AGN. Typically, AGNs also emit in the radio band, if jet-like outflows are observed in the optical band; highly relativistic jets powered by the central black hole could also lead to a  $\gamma$ -ray emitting AGN, or a blazar. For a recent review see Ref. 40. Radio quiet AGNs have some hard x-rays/soft  $\gamma$  rays in their spectra, and their origin is most likely due to accretion.

For blazars, where the jet dominates, polarization measurements in the x- and  $\gamma$ -ray bands can allow us to constrain the morphology and geometry of the emitting region, as well as place constraints on the various proposed emission mechanisms. Typically, the blazar spectra can be described by two broad peaks one in the mm to soft x-ray band, and a second peak in the  $\gamma$ -ray energy range. High levels of polarization for the photons in the low-energy maximum band indicate that synchrotron radiation is a likely source. The high-energy maximum is thought to be due to inverse Compton (IC) of the same synchrotron electrons. Depending on the source for the photon field responsible for the IC effect, the resulting radiation can be polarized, and measurement of polarization can be used to disambiguate between the various “seed” photon fields. For a review of the expected polarization signatures the hard x-ray to soft  $\gamma$  ray energy for blazars, see Ref. 41.

## 3 Photon Polarimetry in Astrophysics Research

Several physical processes, such as the photoelectric effect, Thomson scattering, Compton scattering, and electron-positron pair production can be used to measure photon linear polarization. Polarimeters based on the photoelectric effect and Thomson scattering are used at very low energies. Compton polarimeters are commonly used for energies from 50 keV to a few MeV.<sup>17–22</sup> Those polarimeters are not efficient at a photon energy of 100 MeV because kinematical suppression of the Compton rate at large scattering angles leads to a fast drop in the analyzing power (as  $1/E_\gamma$ ) above the energy range of a few MeV.

Some of the major achievements in astrophysics that were obtained using polarimetry are the discovery of synchrotron radiation from the crab nebula,<sup>42</sup> the study of the surface composition of solar system objects,<sup>43</sup> the measurement of the x-ray linear polarization of the crab nebula,<sup>44</sup> which is still one of the best measurements of linear polarization for astrophysical sources, mapping of solar and stellar magnetic fields,<sup>45</sup> detection of polarization in the CMB radiation,<sup>46</sup> and analysis of large-scale galactic magnetic fields.<sup>47</sup>

The measurement of polarization in this high-energy  $\gamma$  ray regime can be done by detecting the electron-positron pairs produced by  $\gamma$  rays and analysis of a nonuniformity of event distribution in the electron-positron pair plane angle, as discussed in Refs. 48 and 49. However, implementation of this technique should consider limitations due to multiple Coulomb scatterings in the detector, and there are no successful polarization measurements for astrophysical sources in the energy regime of interest in our paper.

A number of missions have included cosmic  $\gamma$ -ray observations, but only a few of them are capable of measuring polarization. The polarimetry measurements were mainly restricted to  $\gamma$  rays with low energies  $E < 10$  MeV. As an example,

the Reuven Ramaty High-Energy Solar Spectroscopic Imager (RHESSI),<sup>50</sup> launched to image the Sun at energies from 3 keV to 20 MeV, was capable of polarimetry up to 2 MeV, and the results were successfully used to study the polarization of numerous solar flares.<sup>51,52</sup>

The SPI detector INTErnational Gamma-Ray Astrophysics Laboratory (INTEGRAL) instrument<sup>53</sup> has the capability of detecting polarization in the range of 3 keV to 8 MeV.<sup>17,54</sup> It was used to measure the polarization of GRB 041219a, and later a high degree of polarization of  $\gamma$  rays from that source<sup>55,56</sup> was confirmed. The tracking and imaging Gamma ray experiment Compton telescope, which observes  $\gamma$  rays in the range of 0.1 to 100 MeV, can measure polarization up to 2 MeV.

Recently, Morselli et al.<sup>57</sup> proposed GAMMA-LIGHT to detect  $\gamma$  rays in the energy range 10 MeV to 10 GeV, and they believe that it will provide solutions to all the current issues that could not be resolved by AGILE and FERMI-LAT in the energy range 10 to 200 MeV. It can also determine the polarization for intense sources of energies above a few hundred MeV with high accuracy.

In spite of the limitations due to low sensitivity, there are numerous polarimetry studies in  $\gamma$  ray astrophysics, and various proposals have been put forth regarding medium- and high-energy  $\gamma$  ray polarimeters. In addition to the ones already mentioned in the Introduction, we briefly discuss here some other important proposals. For example, Blosler et al.<sup>12</sup> proposed the Advanced Pair Telescope (APT), also a polarimeter, in the  $\sim 50$  MeV to 1 GeV range. That proposal uses a gas-based TPC with microwell amplification to track the  $e^+$ ,  $e^-$  paths. The polarization sensitivity was estimated using Geant4 Monte Carlo simulations. Preliminary results indicated that it will be capable of detecting linearly polarized emissions from bright sources at 100 MeV. As an updated version of the APT, Hunter et al.<sup>15</sup> suggested the AdEPT for  $\gamma$ -ray polarimetry in the medium energy range; further, they mentioned that it would also provide better photon angular resolution than FERMI-LAT in the range of  $\sim 5$  to  $\sim 200$  MeV.

HARPO is a hermetic argon TPC detector proposed by Bernard and Delbart,<sup>13,14</sup> which would have high angular resolution and would be sensitive to polarization of  $\gamma$  rays with energies in the MeV to GeV range. A demonstrator for this TPC was built, and preliminary estimates of the spatial resolution are encouraging. Currently, the HARPO team is finalizing a demonstrator set up to characterize a beam of polarized  $\gamma$  rays in the energy range of 2 to 76 MeV.<sup>58</sup>

## 4 Photon Flux from the Crab System

Below we discuss the importance of  $\gamma$  ray polarimetry studies for the crab pulsar/nebula system. After the initial finding of polarization in the  $\gamma$  ray flux from the crab nebula, reported in Ref. 59 when analyzing the data from the spectrometer on INTEGRAL, and its subsequent confirmation in Ref. 60, a series of more detailed studies followed, to constrain the parameters for the main emission mechanisms. For example, observations of the  $\gamma$  rays from the crab pulsar and crab nebula have been reported in Ref. 61 for 8 months of survey data with FERMI-LAT. The pulsar dominates the phase-averaged photon flux, but there is an off-pulse window (the phase interval between  $\sim 0.5$  and  $\sim 0.8$  of the pulsar period, lasting about 35% of the total duration of the cycle) when the pulsar flux is negligible, and it is therefore possible to observe the nebular,

highly polarized, emission. To determine the polarization fraction and polarization angle for the crab pulsar/nebula and similar systems, one starts from the azimuthal profile  $N(\psi)$  in Compton counts, which can be parametrized as follows:

$$N(\psi) = S[1 + a_0 \cos(2\psi - 2\psi_0)], \quad (1)$$

for a source with polarization angle  $PA = \psi_0$  and polarization fraction  $PF = a_0/a_{100}$ . The amplitude  $a_{100}$  corresponds to the measured amplitude for a 100% polarized source. The crab system is an excellent candidate for studying  $\gamma$  ray polarization, and for calibrating any future instruments, since the phase-averaged PF in the 300 to 450 keV band is  $98\% \pm 37\%$  (see Ref. 62), and in the 0.1- to 1-MeV band the PF is  $46\% \pm 10\%$  (see Ref. 59).

According to the analysis conducted in Ref. 61, the spectrum of the crab nebula in the 100 to 300 MeV range can be described by the following combined equation:

$$\frac{dN}{dE} = N_{\text{sync}} E^{-\Gamma_{\text{sync}}} + N_{\text{IC}} E^{-\Gamma_{\text{IC}}}, \quad (2)$$

where the quantity  $dN/dE$  is measured in  $\text{cm}^{-2} \text{s}^{-1} \text{MeV}^{-1}$  representing the number of photons reaching  $1 \text{ cm}^2$  of the detector area per second, per 1 MeV of energy. The energy  $E$  on the right-hand side is measured in GeV. The prefactors  $N_{\text{sync}} \approx 9.1 \times 10^{-13} \text{ cm}^{-2} \text{s}^{-1} \text{MeV}^{-1}$  and  $N_{\text{IC}} \approx 6.4 \times 10^{-12} \text{ cm}^{-2} \text{s}^{-1} \text{MeV}^{-1}$  are determined by 35% of the total duration of the cycle, whereas  $\Gamma_{\text{sync}} \approx 4$  and  $\Gamma_{\text{IC}} \approx 1.65$ . The first and second terms on the right-hand side, as well as the indices “sync” and “IC,” correspond to the synchrotron and IC components of the spectrum, respectively. As one can see, these terms have different dependence on the energy  $E$  as they represent different contributions to the total spectrum. The first part (the synchrotron radiation) comes from emission by high-energy electrons in the nebular magnetic field, whereas the second part is due to the IC scattering of the primary accelerated, relativistic, electrons off of the various soft “seed” photon fields present such as the synchrotron, far infrared excess, and CMB (see Ref. 63 for the fourth possible source of “seed photons”). Polarization measurements could potentially be used to disambiguate between those various “seed” fields, in a similar manner to the case of blazars discussed in Sec. 2.3.

For convenience, let us rewrite the equation for the spectrum of the crab nebula in the following form:

$$\frac{dN}{dE} = \tilde{N}_{\text{sync}} E^{-\Gamma_{\text{sync}}} + \tilde{N}_{\text{IC}} E^{-\Gamma_{\text{IC}}}, \quad (3)$$

where the energy  $E$  on both sides is now measured in MeV; therefore,  $\tilde{N}_{\text{sync}} \approx 9.1 \times 10^{-1} \text{ cm}^{-2} \text{s}^{-1} \text{MeV}^{-1}$  and  $\tilde{N}_{\text{IC}} \approx 5.7 \times 10^{-7} \text{ cm}^{-2} \text{s}^{-1} \text{MeV}^{-1}$ . Integrating  $dN/dE$ , for the photon flux above 100 MeV coming from the crab nebula we obtain the number  $\sim 3.5 \times 10^{-7} \text{ cm}^{-2} \text{s}^{-1}$ , giving for the total cycle duration  $\sim 10^{-6} \text{ cm}^{-2} \text{s}^{-1}$ , or  $\sim 3 \times 10^5 \text{ m}^{-2} \text{y}^{-1}$ .

At the same time, the averaged spectrum of the crab pulsar is described in Ref. 61 as follows:

$$\frac{dN}{dE} = N_0 E^{-\Gamma} \exp\left(-\frac{E}{E_c}\right), \quad (4)$$

where  $N_0 \approx 2.36 \times 10^{-4} \text{ cm}^{-2} \text{s}^{-1} \text{MeV}^{-1}$ ,  $\Gamma \approx 2$ , and the cut-off energy  $E_c \approx 5800 \text{ MeV}$ . As before, the energy  $E$  on both sides is measured in MeV. Integrating this equation, for the

photon flux above 100 MeV coming from the crab pulsar, we obtain the number  $\sim 2 \times 10^{-6} \text{ cm}^{-2} \text{s}^{-1}$  or  $\sim 6 \times 10^5 \text{ m}^{-2} \text{y}^{-1}$ . Thus, the Pulsar’s photon flux is twice as intensive as the nebula’s. A fast photometer could be added to the polarimeter instrumentation to collect events and have a temporal tag and consequently distinguish between nebula and pulsar photons, see, e.g., Refs. 64–66.

We will use the numbers above for an estimation of the polarimeter results at a 100-MeV energy cut. For a 500-MeV cut, the number of events drops by a factor of five (because  $E_c$  is much higher than the exponential factor that does not play a role).

It is worth noting that the estimates following from Ref. 61 approximately agree with the corresponding estimates made in Ref. 67 [where the Eqs. (1) and (2) describe the synchrotron and IC components of the crab nebula spectrum, whereas the Eq. (3) describes the averaged crab pulsar spectrum]. According to Ref. 67, the total crab nebula photon flux above 100 MeV is  $\sim 7.2 \times 10^{-7} \text{ cm}^{-2} \text{s}^{-1}$ , whereas for the crab pulsar the value again reads  $\sim 2 \times 10^{-6} \text{ cm}^{-2} \text{s}^{-1}$ .

## 5 Photon Polarimetry with Pair Production

The photo production of an electron-positron pair in the field of nuclei is a well-understood process that was calculated in QED with all details including the effect of photon linear polarization, see, e.g., Refs. 68 and 69. The kinematics and variables of the reactions are shown in Fig. 1. The distribution of events over an azimuthal angle  $\phi_{+(-)}$  of a positron (electron) relative to the direction of an incident photon has the following form:

$dN/d\phi_{\pm} \propto 1 + A \cdot P_{\gamma} \cdot \cos 2[\phi_{+(-)} + \Delta]$ , where  $A$  is the analyzing power,  $P_{\gamma}$  is the degree of the photon linear polarization, and  $\Delta$  is the angle of the photon linear polarization vector in the detector coordinate system, respectively. In practice,<sup>70</sup> angle  $\omega_{\pm}$  could be used instead of  $\phi_{+(-)}$  because at the photon energies of interest the coplanarity angle is  $\phi_{\pm} \sim 180$  deg.

The value of analyzing power  $A$  was found to be a complicated function of the event parameters and detection arrangement.<sup>68,69</sup> The numerical integration of the full equation could be performed for given conditions, see, e.g., Ref. 70. In a high-energy limit, a compact equation for the integrated

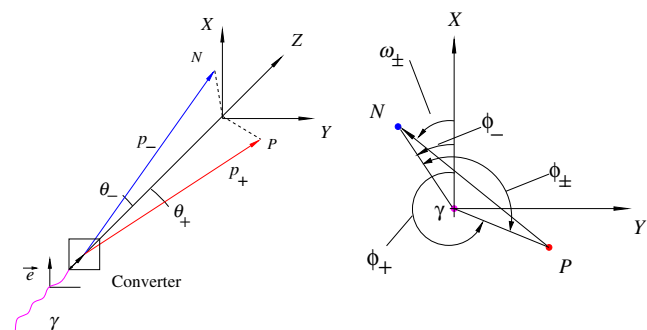


**Fig. 1** The kinematics of  $e^+e^-$  pair photo production (left picture) and the azimuthal angles in the detector plane from Ref. 70. The photon momentum is directed along the Z-axis. The photon polarization vector  $\vec{e}$  is parallel to the x-axis. The angle  $\phi_+$ ,  $\phi_-$  is the angle between the photon polarization plane and the plane constructed by the momentum of the photon and the momentum of the positron (the electron). The angle  $\phi_{\pm}$  is called the coplanarity angle. The labels  $P$  and  $N$  indicate the positions of the crossings of the detector plane by the positron and the electron. The azimuthal angle  $\omega_{\pm}$  between the polarization plane and the vector  $\vec{PN}$  is a directly measurable parameter.

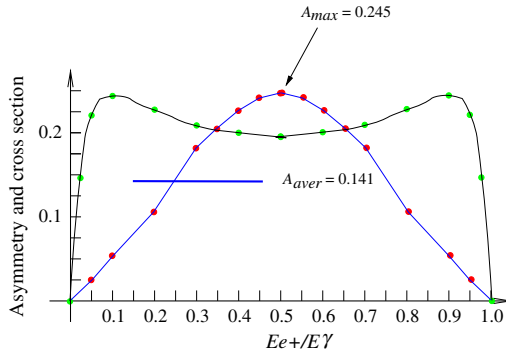


**Fig. 2** The asymmetry (red dots) and cross section (green dots) of pair production by 2 GeV 100% linearly polarized photons as a function of positron energy.<sup>70</sup>  $A_{\text{aver}}$  shows the asymmetry averaged over the full range of the positron energy.

analyzing power for the pair photo-production from atomic electron was obtained in Ref. 71.

The practical design and the test of the polarimeter for a beam of high-energy photons were reported in Ref. 72. There, we detected both particles of the pair and reconstructed the azimuthal angle of the pair plane  $\omega_{\pm}$  (see Fig. 1). The analyzing power, averaged over energy sharing between electron and positron and pair open angle of the experimental acceptance, has been found to be  $0.116 \pm 0.002$ , comparable with a 0.14 value as shown in Fig. 2 reproduced from Ref. 70. When the pair components move through the converter, the azimuthal angle built on pair coordinates and pair vertex becomes blurred due to multiple scattering.

It is useful to note that the purpose of development in Ref. 72 was a polarimeter for an intense photon beam. The thickness of the converter in the beam polarimeter was chosen to be very small to minimize systematics of the measurement of the photon polarization degree. However, the polarimeter could be calibrated using the highly polarized photon beams produced in the laser-backscattering facilities. For the cosmic ray polarimeter, we propose a larger converter thickness and calibration of the device. Such an approach is more productive for cosmic rays studies, where a relative systematic error on the polarization degree at the level of 3% to 5% is acceptable.

Let us also note that for the photon beam polarimetry there are additional options such as a coherent pair production in an oriented crystal and a magnetic separation of the pair components used many years ago in nuclear physics experiments. For the spaceborne photon investigation, those polarimeters are not applicable for the obvious reasons of the limited angle range for the coherent effects and the large weight and power consumption of the magnetic system.

An active converter with a coordinate resolution of a few microns would allow us to construct a dream device, a very efficient polarimeter. A real-world active-converter device, a gas-filled TPC, has a spatial resolution of 100  $\mu\text{m}$  and much larger two-track resolution of 1.5 to 2 mm (for a few cm long drift distance). Such a polarimeter will be a very productive instrument for the photon energy range below 50 MeV. However, because of these resolutions, it would be hard to measure the degree of polarization of photons whose energy is greater than 100 MeV.

A polarimeter with a separation of the converter and pair detector functions could benefit from the high coordinate resolution of the silicon MSD of 10 to 15  $\mu\text{m}$ , its two-track

resolution of 0.2 mm, and flexibility of the distance between a converter and pair hits detector: between them would be a vacuum gap.

## 6 Polarimeter for Cosmic $\gamma$ Rays

The key parameters of the polarimeter are the efficiency,  $\epsilon$ , and analyzing power,  $A$ . Here we outline the analysis of the figure-of-merit,  $\text{FOM} = \epsilon \times A^2$ . We will consider a polarimeter as a stack of individual flat cells, each of which is composed of a converter with a two-dimensional coordinate readout and a coordinate detector for two-track events with no material between them.

The thickness of the converter, where the photon produces the electron-positron pair, defines in the first approximation of the polarimeter efficiency as follows:

$$\epsilon = \eta_{\text{cell}} \times \frac{1 - r^n}{1 - r}. \quad (5)$$

The efficiency of one cell is  $\eta_{\text{cell}} = 1 - \exp(-\frac{7}{9} \times t_{\text{conv}})$ , where  $t_{\text{conv}}$  is the thickness of the converter in units of radiation length. The  $r$  is the reduction of the photon flux due to absorption in a single cell defined as  $r = \exp(-\frac{7}{9} \times t_{\text{cell}-r})$ , where  $t_{\text{cell}-r}$  is the thickness of the cell in units of radiation length, and  $n = L/t_{\text{cell}-g}$  is the number of cells in the device of length  $L$  and geometrical thickness of the cell  $t_{\text{cell}-g}$ .

The converter thickness needs to be optimized because above some thickness it does not improve the FOM or the accuracy of the polarimeter result (see Sec. 7). As it is shown in Fig. 2, selection of the symmetric pairs ( $E_+ = E_-$ ) provides an analyzing power  $A_{\text{sim}} = 0.25$ , whereas the analyzing power averaged over pair energy sharing  $A_{\text{aver}} = 0.14$ . However, the value of the FOM is largest when the cut on pair energy sharing is relaxed. The practical case for the energy cut is  $E_+, E_- > E_{\gamma}/4$ , which allows us to avoid events with a low value of  $A$  and most  $\delta$ -electron contamination. The average value of  $A$  for such a range of  $e^+ - e^-$  energy sharing is 0.20.

The energy of the particles and the shower coordinates could be measured by a segmented electromagnetic calorimeter or estimated from the width of the track, which, due to multiple scattering, is inversely proportional to the particle momentum. In the photon energy range of interest, both electron and positron will pass through a large number of cells. Determination of particle energy based on multiple scattering would provide  $\sim 20\%$  relative energy resolution, which is sufficient for the proposed cut  $E_+, E_- > E_{\gamma}/4$ . Estimation of the particle energy could also be useful for rejection of the hits in MSDs induced by the  $\delta$ -electrons.

## 7 Monte Carlo Simulation

A Monte Carlo simulation was used to evaluate the general effects of pair production in the converter and the specific design of the polarimeter.

### 7.1 Study of the Converter Thickness Effects

We used a Geant3-based MC code to study the photon detection efficiency and electron-positron pair azimuthal distribution in a wide range of converter thickness up to 10% of radiation length. Because both the pair opening angle and multiple scattering are scaled with the photon energy, the distributions are almost energy independent. We present first the results for 100-MeV photon energy for different thicknesses of the converter at

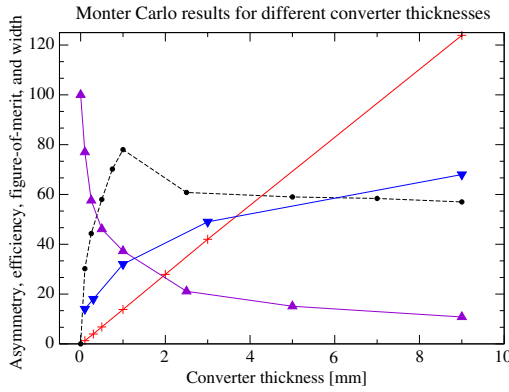


**Fig. 3** Results of MC simulation for 100-MeV photon energy versus thickness of the converter. The purple set (triangles pointing upward) is for the analyzing power (normalized to the value 0.20 at the conversion point). The red set (crosses) is the number of  $e^+e^-$  pairs with  $E_+, E_- > E_\gamma/4$  per  $2 \times 10^4$  incident photons. The blue set (triangles pointing downward) is for the rms of the difference  $\Delta\omega_\pm$  between the angle  $\omega_\pm$  at the production point and at the detector. The  $\Delta\omega_\pm$  shows a loss of correlation between production and detection points, in units of 10 mrad. The black set (circles) is the FOM =  $\epsilon \times A^2$  in arbitrary units. A cut  $r_{+-} > 0.2$  mm was applied on the distance between coordinates of two tracks (for 20 mm between the converter and the detector planes).

a fixed distance of 20 mm between the converter end and the detector.

We used a standard Geant3 pair production generator for the unpolarized photons and at the conversion point introduced a weighting factor for each event as  $W(\omega_\pm) = 1 + A \cos 2\omega_\pm$  to simulate a polarization effect on an event-by-event basis. The value of azimuthal angle modulation at the pair production point was fixed at 0.20, which is the average value of the analyzing power  $A$  at production over the selected range of particle energies. The pair component propagation was realized in the MC, and the track parameters were evaluated.

Figure 3 shows the summary of MC results. The apparent optimum converter thickness is close to 1 mm, for which the projected  $A = 0.10$  is reasonably large and the FOM is close to the saturation limit. However, we are expecting that when  $\delta$ -electron hits are included in analysis the optimum thickness for the 100-MeV photon case will be smaller and the FOM will be a bit lower.

## 7.2 Detector Parameters

The coordinate detector allows determination of the opening angle between the pair components and the azimuthal angle of the pair plane relative to the lab coordinate system, the main variable for measurement of the photon polarization. Such a detector is characterized by the coordinate resolution,  $\sigma_x$ , and the minimum two-track distance,  $a_{x,\min}$ , at which coordinates of two tracks could be determined with quoted  $\sigma_x$  accuracy. The  $a_{x,\min}$  is typically 2 mm for the drift chamber. For TPC with a micromega amplification stage and a strip-type readout,  $a_{x,\min}$  is about four strips or 1.6 mm (pitch equal to 400  $\mu\text{m}$ ). For silicon MSD,  $a_{x,\min}$  is about 0.20 mm (pitch equal to 50  $\mu\text{m}$ ).

The opening angle between the pair components is on the order of  $4/(E_\gamma/m_e)$ , where  $E_\gamma$  is the photon energy and  $m_e$  is the electron rest mass. The events with an opening angle larger than  $3/(E_\gamma/m_e)$  but  $< 9/(E_\gamma/m_e)$  provide most of the analyzing power, as it is shown in Ref. 70. It is easy to find

**Table 1** The geometrical cell thickness,  $t_{\text{cell-g}}$ , in cm for the different detectors and photon energies.

Photon energy [MeV]	Drift chamber	TPC/micromega	Silicon MSD
20	2.6	2	0.26
100	13	10	1.3
500	65	52	6.5
2000	260	210	26

that the resulting geometrical thickness of the cell is  $t_{\text{cell-g}} = (a_{x,\min} \cdot E_\gamma)/(3 \cdot m_e)$ , whose numerical values are shown in Table 1.

For photon energies above 100 MeV, the silicon MSD is a preferable option because of the limit on the apparatus's total length. Indeed, considering a 300-cm total length and an energy of 500 MeV, the number of cells is 5 for the drift chamber option, 6 for the TPC/micromega, and 46 for the MSD option. At the same time, the total amount of matter in the polarimeter should be limited to one radiation length or less because of significant absorption of the incident photons, which will reduce the average efficiency per cell. For example, in the MSD option 54% absorption will occur with 46 cells (1-mm thickness 2-D readout converter detector and two 0.3-mm thickness 1-D readout track detectors). The detection efficiency (pair production in the converters) could be estimated as  $\epsilon = \eta_{\text{cell}} \times \frac{1-r}{1+r}$  [Eq. (5)], which is about 34% for the selected parameters of the polarimeter. However, the useful statistics result is lower due to a cut on the pair components' energies and contributions of the nonpair production processes, especially at low photon energy. For a photon energy of 100 MeV, the obtained efficiency is 0.28% per cell and the overall efficiency for the 30 cell polarimeter is 9%. The efficiency becomes significantly larger ( $\sim 15\%$ ) for a photon energy of 800 MeV.

Assuming observation of the crab pulsar photon source with a 1 m<sup>2</sup> detector for 1 year, the total statistics of pairs (above a 100-MeV photon energy cut) was estimated to be  $N_{\text{pairs}} = 6 \times 10^5 \times 0.09 = 0.54 \times 10^5$ . For the projected analyzing power  $A$  of 0.10, the statistical accuracy of the polarization measurement is  $\sigma_P = \frac{1}{A} \times \sqrt{\frac{2}{N_{\text{pairs}}}} \approx 0.10$  for the MSD detector option. Realization of such high accuracy would require a prior calibration of the polarimeter at a laser-back scattering facility.

## 7.3 Geometry of the Microstrip Detectors-Based Polarimeter

The polarimeter is composed of 30 cells. A single cell of the MSD-based polarimeter is composed of two double-sided 1-m  $\times$  1-m wide microstrip detector planes each separated by 20 mm (see Fig. 4). The first plane is 0.3-mm thick and the second is 0.6-mm thick, and they both act as a converter. They determine the coordinates of the gamma annihilation point. In our analysis, we are using an analysis group, which includes four planes. The third and fourth planes of the analysis group are components of adjacent cells. Every other cell has its readout strips rotated by 45 deg with respect to the previous cell planes. As a consequence, one cell and the next in line measure two

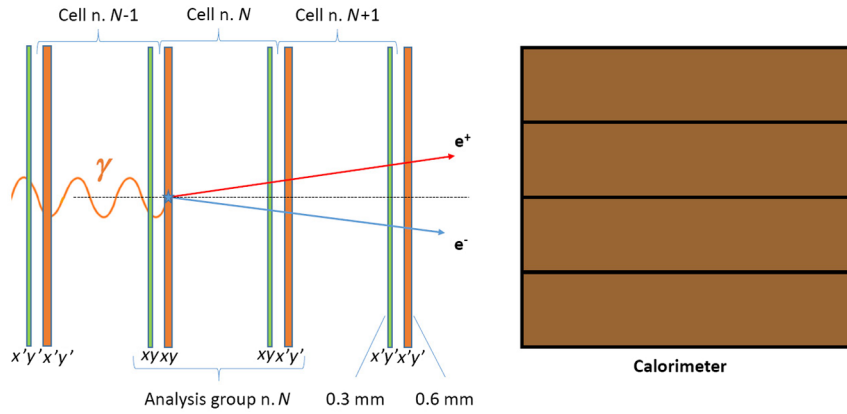


Fig. 4 A schematic 2-D view of three cells and of the calorimeter of the polarimeter.

different sets of coordinates  $[(X, Y)$  and  $(X', Y')$ , respectively]. Measurement of two sets of coordinates allows unambiguous determination of the two-particle event geometry.

To avoid strips that are too long and hence a signal/noise ratio that is too small, each plane is subdivided into four quadrants, electronically independent of each other, made up in turn of a mosaic of  $5 \times 5$  DC-coupled  $100\text{-}\mu\text{m}$  pitch silicon MSDs of dimensions  $10\text{ cm} \times 10\text{ cm}$  (see Fig. 5). On the side of each plane, the strips of the five silicon MSDs forming a row (column) of a quadrant are connected in a series to form five

50-cm-long ladders that detect the  $X/X'$  ( $Y/Y'$ ) track coordinates, respectively. The quadrants are glued to thin kapton foils that electrically insulate them from a carbon-fiber backbone whose thickness is about  $0.5\text{ cm}$  (see Fig. 5). One-side single microstrip detector ladders of this kind as long as  $72\text{ cm}$  have already been built by Ref. 73.

To avoid excessive readout electronic power consumption, the analog signals from each 50-cm-long strip, after being amplified, discriminated by a comparator, and, after being digitally pipelined and encoded, are multiplexed in 128-bit words

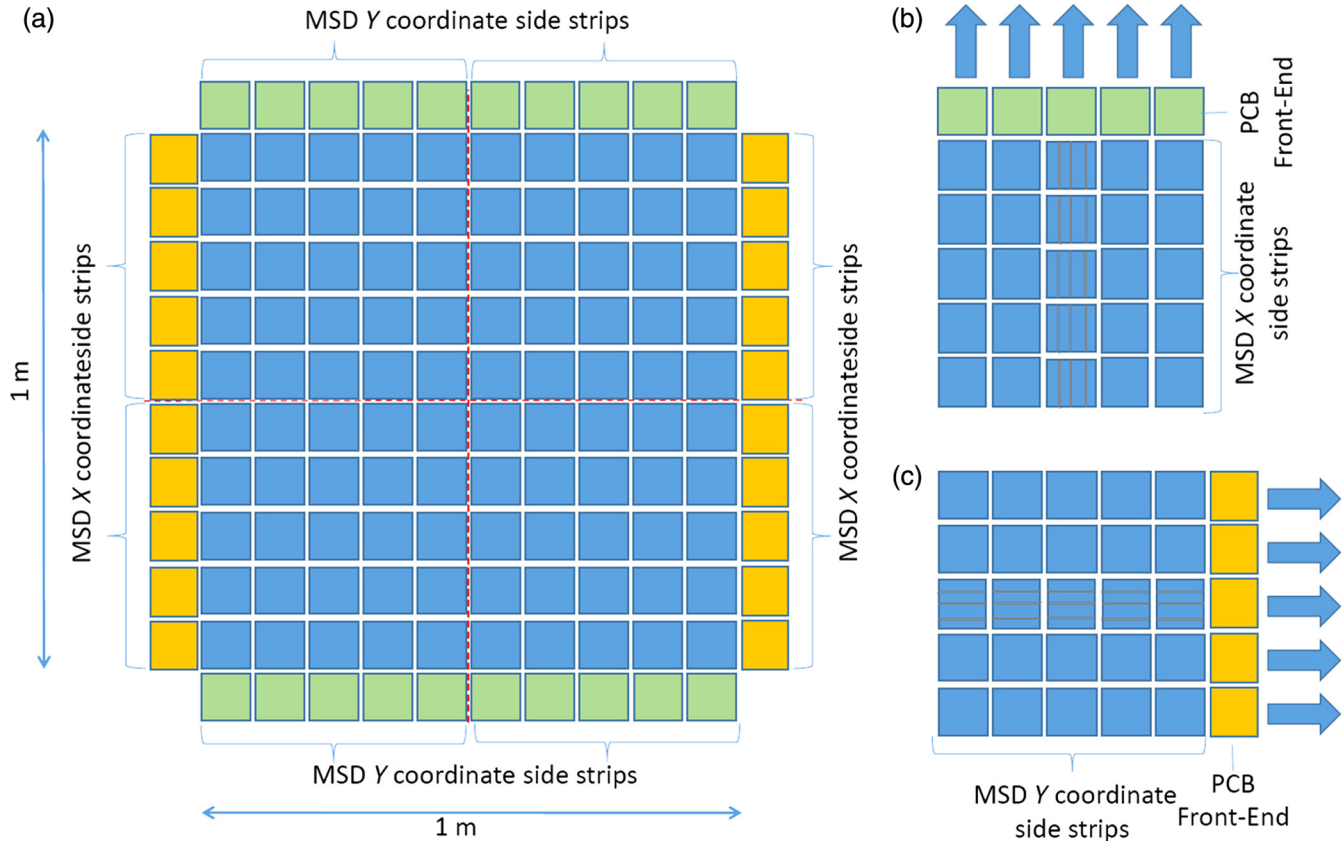


Fig. 5 (a) The schematic front view of a plane made up of its four quadrants, and their read out electronics. In green, the electronics printed circuit boards (PCB) of the X-coordinate side strips. In yellow, the electronics PCB of the Y-coordinate side strips. (b) Front view of a single quadrant X-coordinate side. (c) Front view of a single quadrant Y-coordinate side. Each quadrant is divided into five rows, each formed by connecting five MSDs in a line.

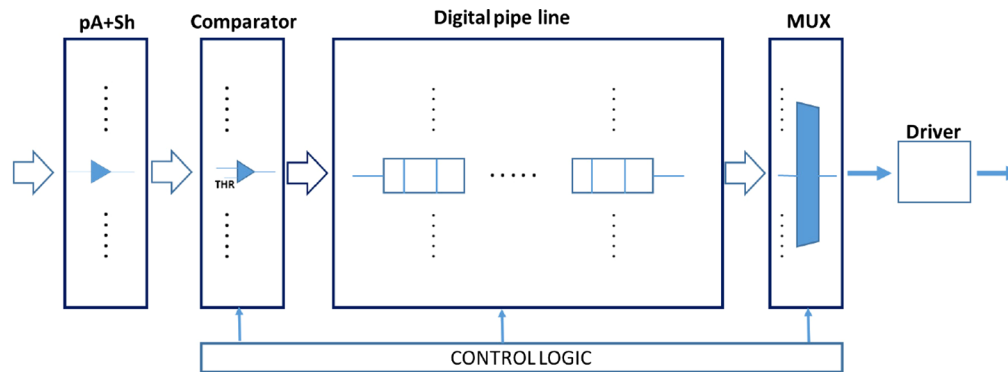


Fig. 6 The layout of the readout electronics.

(see Fig. 6). We calculated a power consumption reduction, with respect to a standard corresponding analog readout, by a factor of six, at least.<sup>74</sup> Considering a standard front end analog readout power consumption of about 1.2 mW/channel and a figure of 2480.000 channels for the polarimeter, this adds up to a power consumption of about 450 W. This value will likely be reduced in the future by the present steady improvement of application-specific integrated circuit Technology. A calorimeter will be used for crude ( $\sim 20\%$ ) measurement of the photon energy (combined energy of the  $e^+e^-$  pair).

## 8 Projected Results and Conclusions

The projected accuracy of polarization measurement is shown in Fig. 7. For each data point, we averaged the incident flux over all energies above the shown value. The photon angular resolution of the proposed system was obtained from MC simulation as  $\sim 5$  mrad for 200-MeV photon energy.

A  $\gamma$  ray polarimeter for astrophysics could be constructed using silicon MSD technology. Each of the 30 cells will include one MSD with 2-D readout of 0.6-mm thickness and one MSD with 2-D readout of 0.3-mm thickness and 0.1-mm pitch. Using a total of 60 m<sup>2</sup> area of MSD (30 cells), the polarimeter would be a device with 9% to 15% photon efficiency and an average analyzing power of 10%. In a year-long observation, the polarization of the photons from the crab pulsar would be measured to 8% accuracy at an energy above 100 MeV and  $\sim 30\%$  accuracy at an energy above 800 MeV.

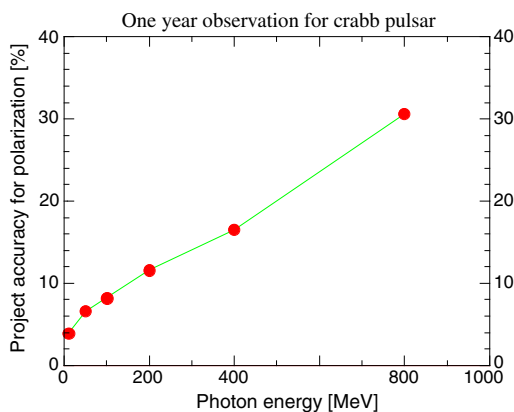


Fig. 7 Projected accuracy of the polarization measurement with the proposed polarimeter for a different level of photon energy cut.

## Acknowledgments

This work was supported by NASA award NNX09AV07A and NSF CREST award HRD-1345219.

## References

1. T. Young, "The Bakerian lecture: on the theory of light and colors," *Philos. Trans. R. Soc. London* **92** 12–48 (1802).
2. A. Michelson and E. Morley, "On the relative motion of the earth and the luminiferous ether," *Am. J. Sci.* **s3-34**, 333–345 (1887).
3. C. N. Yang, "Possible experimental determination of whether the neutral meson is scalar or pseudoscalar," *Phys. Rev.* **77**, 722–723 (1950).
4. J. H. Berlin and L. Madansky, "On the detection of  $\gamma$ -ray polarization by pair production," *Phys. Rev.* **78**, 623–623 (1950).
5. C. Aidala et al., "The spin structure of the nucleon," *Rev. Mod. Phys.* **85**, 655–691 (2013).
6. [sci.esa.int/planck](http://sci.esa.int/planck)
7. M. Kamionkowski and E. D. Kovetz, "The quest for B modes from inflationary gravitational waves," *Ann. Rev. Astron. Astrophys.* **54**, 227–269 (2016).
8. [agile.rm.iasf.cnr.it](http://agile.rm.iasf.cnr.it)
9. [www-glast.stanford.edu](http://www-glast.stanford.edu)
10. M. Gioni et al., "Estimate of the Fermi large area telescope sensitivity to gamma-ray polarization," *AIP Conf. Proc.* **1792**(1), 070022 (2017).
11. P. Laurent et al., "Constraints on Lorentz invariance violation using integral/IBIS observations of GRB041219A," *Phys. Rev. D* **83**, 121301 (2011).
12. P. F. Bloser et al., "The MEGA project: science goals and hardware development," *New Astron. Rev.* **50**, 619–623 (2006).
13. D. Bernard and A. Delbart, "High-angular-precision-ray astronomy and polarimetry," *Nucl. Instrum. Methods Phys. Res. Sect. A* **695**, 71–73 (2012).
14. D. Bernard, "Polarimetry of cosmic gamma-ray sources above  $e^+e^-$  pair creation threshold," *Nucl. Instrum. Methods Phys. Res. Sect. A* **729**, 765–780 (2013).
15. S. D. Hunter et al., "A pair production telescope for medium-energy gamma-ray polarimetry," *Astropart. Phys.* **59**, 18–28 (2014).
16. A. De Angelis et al., "The e-ASTROGAM mission," *Exp. Astron.* **44**(1), 25–82 (2017).
17. F. Lei, A. J. Dean, and G. L. Hills, "Compton polarimetry in gamma-ray astronomy," *Space Sci. Rev.* **82**, 309–388 (1997).
18. M. L. McConnell and J. M. Ryan, "Status and prospects for polarimetry in high energy astrophysics," *New Astron. Rev.* **48**, 215–219 (2004).
19. M. L. McConnell and P. F. Bloser, "Status and future prospects for  $\gamma$ -ray polarimetry," *Chin. J. Astron. Astrophys.* **6**, 237–246 (2006).
20. H. Krawczynski et al., "Scientific prospects for hard x-ray polarimetry," *Astropart. Phys.* **34**, 550–567 (2011).
21. W. Hajdas and E. Suarez-Garcia, "Polarimetry at high energies," in *Observing Photons in Space: A Guide to Experimental Space Astronomy*, M. C. E. Huber et al., Eds., pp. 599–615, Springer, New York (2013).
22. M. Pohl, "Particle detection technology for space-borne astroparticle experiments," *Proc. Sci.* **TIPP2014**, 013 arXiv:1409.1823 (2015).

23. J. Knodlseder, "The future of gamma-ray astronomy," *C. R. Phys.* **17**, 663–678 (2016).
24. M. Dovciak et al., "Thermal disc emission from a rotating black hole: x-ray polarization signatures," *Mon. Not. R. Astron. Soc.* **391**, 32–38 (2008).
25. T. Jacobson, S. Liberati, and D. Mattingly, "Lorentz violation at high energy: concepts, phenomena and astrophysical constraints," *Ann. Phys.* **321**, 150–196 (2006).
26. D. Gotz et al., "GRB 140206A: the most distant polarized gamma-ray burst," *Mon. Not. R. Astron. Soc.* **444**(3), 2776–2782 (2014).
27. [heasarc.gsfc.nasa.gov/docs/cgro/egret](http://heasarc.gsfc.nasa.gov/docs/cgro/egret).
28. O. De Jager et al., "Gamma-ray observations of the crab nebula: a study of the synchro-compton spectrum," *Astrophys. J.* **457**, 253 (1996).
29. S. Komissarov and M. Lyutikov, "On the origin of variable gamma-ray emission from the crab nebula," *Mon. Not. R. Astron. Soc.* **414**, 2017–2028 (2011).
30. V. Rusov et al., "Axion mechanism of sun luminosity: light shining through the solar radiation zone," arXiv:astro-ph/1401.3024 (2014).
31. A. Rubbia and A. Sakharov, "Constraining axion by polarized prompt emission from gamma ray bursts," *Astropart. Phys.* **29**, 20–24 (2008).
32. Y. J. Guo, X. Y. Lai, and R. X. Xu, "A corresponding-state approach to quark-cluster matter," *Chin. Phys. C* **38**(5), 055101 (2014).
33. M. Buballa et al., "EMMI rapid reaction task force meeting on quark matter in compact stars," *J. Phys. G* **41**(12), 123001 (2014).
34. V. M. Kaspi, M. S. E. Roberts, and A. K. Harding, "Isolated neutron stars," in *Compact Stellar X-ray Sources*, W. Lewin and M. Van der Klis, Eds., Cambridge Astrophysics Series, pp. 279–339, Cambridge University Press, Cambridge, UK (2006).
35. M. McConnell et al., "X-ray and gamma-ray polarimetry," in *Astro2010: The Astronomy and Astrophysics Decadal Survey*, Science White Papers no. 198 (2009).
36. P. Meszaros, "Gamma-ray bursts," *Rep. Prog. Phys.* **69**, 2259–2321 (2006).
37. K. Toma et al., "Statistical properties of gamma-ray burst polarization," *Astrophys. J.* **698**, 1042–1053 (2009).
38. C. Mundell et al., "Highly polarized light from stable ordered magnetic fields in GRB 120308A," *Nature* **504**, 119–121 (2013).
39. M. Lyutikov, V. Pariev, and R. D. Blandford, "Polarization of prompt gamma-ray burst emission: evidence for electromagnetically dominated outflow," *Astrophys. J.* **597**, 998–1009 (2003).
40. C. D. Dermer and B. Giebels, "Active galactic nuclei at gamma-ray energies," *C. R. Phys.* **17**, 594–616 (2016).
41. H. Krawczynski, "The polarization properties of inverse compton emission and implications for blazar observations with the gems x-ray polarimeter," *Astrophys. J.* **744**, 30 (2012).
42. J. H. Oort and T. Walraven, "Polarization and composition of the crab nebula," *Bull. Astron. Inst. Neth.* **12**, 285 (1956).
43. E. Bowell and B. Zellner, "Polarizations of asteroids and satellites," in *Planets, Stars, and Nebulae: Studied with Photopolarimetry*, T. Gehrels, Ed., pp. 381–404, University of Arizona Press, Tucson, Arizona (1974).
44. M. C. Weisskopf et al., "A precision measurement of the x-ray polarization of the crab nebula without pulsar contamination," *Astrophys. J.* **220**, L117–L121 (1978).
45. C. J. Schrijver and C. Zwaan, *Solar and Stellar Magnetic Activity*, Cambridge University Press, Cambridge (2000).
46. J. Kovac et al., "Detection of polarization in the cosmic microwave background using DASI," *Nature* **420**, 772–787 (2002).
47. R. M. Kulsrud and E. G. Zweibel, "The origin of astrophysical magnetic fields," *Rep. Prog. Phys.* **71**, 046901 (2008).
48. S. R. Kel'ner, "Dependence of the azimuthal asymmetry of pair-production plane on the photon polarization," *Sov. J. Nucl. Phys.* **10**(3), 349–351 (1970).
49. S. R. Kel'ner, Y. D. Kotov, and V. M. Logunov, "Methods of measuring polarization of gamma quanta," *Sov. J. Nucl. Phys.* **21**(3), 313–315 (1975).
50. [hesperia.gsfc.nasa.gov/rhessi3](http://hesperia.gsfc.nasa.gov/rhessi3).
51. M. L. McConnell et al., "Evidence for hard x-ray polarization from the flare of 23 July 2002," *Bull. Am. Astron. Soc.* **35**, 850 (2003).
52. S. E. Boggs, W. Coburn, and E. Kalemci, "Gamma-ray polarimetry of two x-class solar flares," *Astrophys. J.* **638**, 1129–1139 (2006).
53. [sci.esa.int/integral](http://sci.esa.int/integral).
54. M. Forot et al., "Compton telescope with coded aperture mask: imaging with the INTEGRAL/IBIS Compton mode," *Astrophys. J.* **668**, 1259–1265 (2007).
55. S. McGlynn et al., "Polarisation studies of the prompt gamma-ray emission from GRB 041219a using the spectrometer aboard INTEGRAL," *Astron. Astrophys.* **466**, 895–904 (2007).
56. E. Kalemci et al., "Search for polarization from the prompt gamma-ray emission of GRB 041219a with SPI on INTEGRAL," *Astrophys. J. Suppl.* **169**, 75–82 (2007).
57. A. Morselli et al., "GAMMA-LIGHT: high-energy astrophysics above 10 MeV," *Nucl. Phys. Proc. Suppl.* **239–240**, 193–198 (2013).
58. D. Bernard et al., "HARPO: a TPC as a gamma-ray telescope and polarimeter," *Proc. SPIE* **9144**, 91441M (2014).
59. A. J. Dean et al., "Polarized gamma-ray emission from the crab," *Science* **321**, 1183–1185 (2008).
60. M. Forot et al., "Polarization of the crab pulsar and nebula as observed by the INTEGRAL/IBIS telescope," *Astrophys. J.* **688**, L29–L32 (2008).
61. A. Abdo et al., "Fermi large area telescope observations of the crab pulsar and nebula," *Astrophys. J.* **708**, 1254–1267 (2010).
62. P. Moran et al., "A recent change in the optical and  $\gamma$ -ray polarization of the crab nebula and pulsar," *Mon. Not. R. Astron. Soc.* **456**(3), 2974–2981 (2016).
63. D. Horns and F. A. Aharonian, "The crab nebula: linking MeV synchrotron and 50 TeV inverse Compton photons," *ESA Spec. Publ.* **552**, 439 (2004).
64. F. Meddi et al., "A new fast silicon photomultiplier photometer," *Publ. Astron. Soc. Pac.* **124**(915), 448–453 (2012).
65. F. Ambrosino et al., "SiFAP: a simple sub-millisecond astronomical photometer," *J. Astron. Instrum.* **2**(1), 1350006 (2013).
66. F. Ambrosino et al., "Fast multichannel astronomical photometer based on silicon photo multipliers mounted at the Telescopio Nazionale Galileo," *Proc. SPIE* **9147**, 91478R (2014).
67. R. Buehler et al., "Gamma-ray activity in the crab nebula: the exceptional flare of 2011 April," *Astrophys. J.* **749**, 26 (2012).
68. H. Olsen and L. C. Maximon, "Photon and electron polarization in high-energy Bremsstrahlung and pair production with screening," *Phys. Rev.* **114**, 887–904 (1959).
69. L. C. Maximon and H. Olsen, "Measurement of linear photon polarization by pair production," *Phys. Rev.* **126**, 310–319 (1962).
70. B. Wojtsekhowski, D. Tedeschi, and B. Vlahovic, "A pair polarimeter for linearly polarized high-energy photons," *Nucl. Instrum. Methods Phys. Res. Sect. A* **515**, 605–613 (2003).
71. V. F. Boldyshev and Y. P. Peresun'ko, "Electron-positron pair photoproduction on electrons and analysis of photon beam polarization," *Yad. Fiz.* **14**, 1027–1032 (1971); translation in the *Sov. J. Nucl. Phys.* **14**(5), 576 (1972).
72. C. de Jager et al., "A pair polarimeter for linearly polarized high energy photons," *Eur. Phys. J. A* **19**, 275–278 (2004).
73. G. Barichello et al., "Performance of long modules of silicon microstrip detectors," *Nucl. Instrum. Methods A* **413**, 17–30 (1998).
74. M. Raymond and G. Hall, "CMS microstrip tracker readout at SLHC," Presented at the *Topical Workshop on Electronics for Particle Physics*, Naxos, Greece (2008).

**Maxim Eingorn** received his PhD in theoretical physics from Odessa National University, Ukraine. He is a theoretical physicist working on astrophysics, cosmology, and theory of gravity. Currently, he works as a research associate at North Carolina Central University, USA. His major publications are devoted to multidimensional gravity and cosmological perturbations in the inhomogeneous universe.

**Lakma Fernando** is a theoretical physicist working on nuclear astrophysics. She pursued her PhD in applied physics from Mississippi State University, USA. Her major publications are devoted to testing effective field theory for low-energy nuclear interactions.

**Branislav Vlahovic** is the director of the National Science Foundation Computational Center of Research Excellence, NASA University Research Center for Aerospace Device, and Department of Homeland Security Center on Detectors and Sensors. In 2004, he was awarded by the Board of Governors of the University of North Carolina the Oliver Max Gardner statewide award for his research and contribution to science. He has published more than 300 research papers in peer-reviewed journals.

**Cosmin Ilie** received his PhD in physics from the University of Michigan in Ann Arbor, where he was an advisee of Prof. K. Freese. He is a theoretical physicist whose research covers a variety of topics in cosmology and astrophysics, with particular emphasis on indirect observational signals for dark matter. Currently, he is a lecturer and research affiliate at Colgate University and maintains research affiliations with UNC Chapel Hill and IFIN-HH in Bucharest.

**Bogdan Wojtsekhowski** received his PhD in experimental nuclear physics from Budker Institute, Russia. He is an experimental physicist working on hadron physics, dark matter detection, particle detectors, and one-way speed of light anisotropy. Currently, he works as a senior staff scientist at the Thomas Jefferson National Accelerator Facility in Newport News, Virginia, USA. His major publications are on the nucleon electromagnetic form factors and mechanism of wide-angle Compton scattering.

**Guido Maria Urciuoli** is a physicist of the Italian National Institute of Nuclear Physics (INFN), and he is the spokesperson of the Italian collaboration at TJNAF. Currently, he is involved as spokesperson, among other experiments, in research aimed at predicting important features of neutron stars like their crust thickness, the way of cooling, the presence of exotic states in their cores (experiment PREX), and at solving the hyperon puzzle (several hypernuclear spectroscopy experiments).

**Fulvio De Persio** received his PhD in experimental physics from the Università di Siena, Italy. He is an experimental physicist working on astrophysics and nuclear physics. Currently, he works as parts engineer at Thales-Alenia Space, Italy. His major publications are devoted to the study and development of detector devices for nuclear physics and astrophysics measurements.

**Franco Meddi** is an experimental physicist, associate professor at Sapienza University of Rome (Italy). He is active in nuclear and elementary particle physics in experiments at LHC at CERN (Geneva, Switzerland) and at SBS at Jefferson Laboratory (Virginia, USA), contributing to the development and implementation of silicon detectors and related electronics. Currently, he is collaborating with a group of astrophysics realizing a silicon fast photometer (SiFAP) devoted to measure pulsars.

**Vladimir Nelyubin** received his PhD in physics of nuclei and particles at Leningrad Nuclear Physics Institute of Academy of Science of USSR in 1983. He is a senior research scientist in the Physics Department at the University of Virginia. At present his research is focused on investigation into the structure of the nucleon and nuclei and developing polarized targets and detectors. His recent publications are devoted to experiments on the electron accelerator of Jefferson Laboratory.